Interfacial Dzyaloshinskii-Moriya interaction induced nonreciprocity of spin wave in magnonic waveguides

Fusheng Ma*[a] and Yan Zhou[bc]

[a]*Temasek Laboratories, National University of Singapore, Singapore 117411, Singapore. E-mail: tslmaf@nus.edu.sg and Fusheng.Ma@gmail.com*

[b]*Department of Physics, The University of Hong Kong, Hong Kong, P. R. China*

[c]*Center of Theoretical and Computational Physics, Univ. of Hong Kong, P. R. China*

E-mail: yanzhou@hku.hk

Abstract

The nonreciprocal propagation of spin waves in magnonic waveguides is investigated using micromagnetic simulations. The magnonic waveguides are in the form of ferromagnet/normal metal bilayers inducing interfacial Dzyaloshinskii-Moriya interaction (DMI). The presence of the interfacial DMI is demonstrated to induce the nonreciprocity of spin waves, i.e. different frequencies, amplitudes, and mode profiles for propagating in the opposite directions. In addition our simulation reveals the existence of unidirectional propagation of spin wave which travels only along one direction, either forward or backward. Our results therefore show the potential of using magnonic waveguides with the presence of DMI as building blocks for a new class of compact nonreciprocal magnonic devices including one-way waveguides (isolators) and circulators.

Keywords: Nonreciprocity, Dzialoshinskii-Moriya interaction, Magnonic Crystal, Magnonics, Spin Wave, Waveguide, Micromagnetic Simulations.

PACS numbers: 75.40.Gb, 75.30.Ds, 75.78.Cd, 75.78.-n

The Dzyaloshinskii-Moriya interaction (DMI), [1, 2] a novel antisymmetric exchange coupling, has recently attracted great interest. The DMI arises from spin-orbit scattering of electrons in an inversion asymmetric crystal field, and it exists in systems with broken inversion symmetry [3-7] and at the surface or interface of magnetic multi-layers. [8-10] The existence of DMI can induce chiral spin structures such as skyrmion, [3-10] unconventional transport phenomena, [11-13] and exotic dynamic properties, [14-16] many of which stimulated interest in fundamental magnetism studies and provided new possibilities for the development of future spintronic devices. Existence of DMI in systems such as Pt/Co with perpendicular magnetic anisotropy (PMA) has been demonstrated from measuring the static profiles of domain walls and their dynamics. [17-20] It has been theoretically predicted that the presence of DMI will result in asymmetry of magnon (the quanta of spin wave) energies propagating in the counter-propagation directions in ultrathin films. [21-24] This nonreciprocity has also been experimentally demonstrated in ultrathin Fe film grown on W(110). [25, 26] Recently, Moon *et al.* have numerically shown that introducing a DMI term into the energy terms will lead to the nonreciprocity of spin wave (SW) that propagates along the positive and negative axis directions, *i.e.* $f(+k) \neq f(-k)$ for an uniformly magnetized infinite planar film. [27] Nonreciprocal propagation of spin waves is of great interest to both fundamental science and engineering applications, since it can be exploited for functionality enhancement or development. For instance, logic devices based on nonreciprocal properties of SWs can be designed with the amplitude modulation for logic operations. [28]

The recent development of nanotechnology together with the advances in nanomagnetics has made it possible for the investigation of spin waves in artificial magnonic crystals (MCs). MCs are magnetic materials with periodic modulated magnetic properties. Their potential application in functional devices has ignited a novel research field, magnonics, aiming to use SWs propagation in a magnetic medium for signal transmission and processing. [29-31] Due to their potential integration with semiconductor technology, magnonics has attracted widespread interest for numerous fields of nanoscience and nanotechnology. [32] Similar to plasmonics which uses metallic nanostructures to confine and guide optical frequency plasmon-polaritons, [33, 34] magnonics utilizes nanoscale magnonic waveguides to control the propagation of SWs. [35] Although the SW propagation in magnonic

waveguides has been widely investigated, [36, 37] the effect of DMI on SWs in such waveguides has not been studied yet.

In this work, we present the effect of interfacial DMI on the spin dynamics and in particular on the spin wave dispersion relation in magnonic waveguide. Micromagnetic simulations are carried out to investigate the interfacial DMI induced nonreciprocal propagation of spin waves in single-component and bi-component magnonic waveguides. Here, an ultrathin ferromagnetic nanostrip providing a well-defined magnonic waveguide is used to study the propagation properties of spin wave in the Damon–Eshbach (DE) geometry. [38] In this geometry, the external magnetic field **H** is applied in the plane of the thin film and the wave vector of the propagating SW is perpendicular to this field.

The schematic of the investigated magnonic waveguides are shown in Figs. 1(a) and (b) for the single-component and bi-component waveguides, respectively. The waveguides are assumed to be in the form of an ultrathin ferromagnetic layer on a metallic substrate inducing DMI. The length of the waveguide is 2000 nm, the width is 400 nm, and the thickness of the ferromagnetic layer is 1 nm. For the single-component magnonic waveguide (SMW) as shown in Fig. 1(a), the ferromagnetic layer is the cobalt (Co) film of 1 nm thickness. While for the bi-component magnonic waveguide (BMW) as shown in Fig. 1(b), the 1nm thick ferromagnetic layer comprises of an alternating array of Co and Permalloy (Py) stripes with a period $a = a_1 + a_2 = 24$ nm ($a_1 = a_2 = 12$ nm). The dispersion relation of SW in terms of the frequency versus wavevector is numerically investigated.

The effect of the DMI on the SW propagation property is simulated using the public object-oriented micromagnetic framework (OOMMF) code including the extension module of the Dzyaloshinskii-Moriya interaction. [39, 40] The code performs a time integration of the Landau-Lifshitz-Gilbert equation of motion for the magnetization dynamics,

$$\frac{\partial \boldsymbol{m}}{\partial t} = -|\gamma_0|[\boldsymbol{m} \times \boldsymbol{H}_{eff}] - \alpha(\boldsymbol{m} \times \frac{\partial \boldsymbol{m}}{\partial t}) \quad (1)$$

where $\boldsymbol{m}$ is the unit vector along the local magnetization, γ_0 is the gyromagnetic ratio, α is the Gilbert damping constant, and $\mathbf{H}_{eff}$ is the local effective magnetic field including the exchange, anisotropy, magnetostatic, and Dzyaloshinskii-Moriya fields.

The Dzyaloshinskii-Moriya field caused by the interfacial DMI is given in a continuous form: [40, 41]

$$\boldsymbol{H}_{DM} = -\frac{2D}{\mu_0 M_s}(\boldsymbol{\nabla} \times \boldsymbol{m}) \tag{2}$$

where D is the continuous effective DMI constant in mJ/m^2, μ_0 is the magnetic permeability, and M_s is the saturation magnetization.

Parameters used in the simulations are listed as follows: the saturation magnetization M_s = 1.752 × 10^6 A/m, the exchange stiffness A = 2.1 × 10^{-11} J/m, and perpendicular magnetic anisotropy K = 0.8 MJ/m^3 for Co, and M_s = 1.94 × 10^5 A/m, A = 4.0 × 10^{-12} J/m and K = 0 for Py. The intensity of the DMI is presented by D in the unit of mJ/m^2. In this work, the DMI constant D = 3 mJ/m^2, the damping constant α = 0.01, and the gyromagnetic ratio γ = 2.211 × 10^5 m/As. The cell size used in the simulation is 1 × 1 × 1 nm^3, which is well below the characteristic wall length of these materials. A static in-plane magnetic field **H** = 100 mT is applied to magnetize the waveguide along the y-direction which is large enough to make the magnetization uniform and minimize the edge effects. The propagation of the SW along the length of the waveguide (x-direction) corresponds to the DE geometry. [38] In order to excite SWs, a cardinal sin function, $H_y(t) = H_0 sin(2\pi\omega_H t)/(2\pi\omega_H t)$, with H_0 = 10 mT and field frequency ω_H = 60 GHz, was applied locally to a 2 × 400 × 1 nm^3 central section of the magnonic waveguides. In this case, the wavevector k of SWs on the right part is positive whereas k is negative on the left part. SWs with frequencies ranging from 0 to 60 GHz were thus excited and propagated along the waveguide. The dispersion curves are obtained by performing the Fourier transformation of the out-of-plane magnetization component m_z in space and time with contributions from all the discretized cells. The mode profile of each SW is then obtained by plotting the spectral amplitude at a specific frequency for each cell. Although the micromagnetic simulations were carried out at room temperature, the presented results are convincing with the presence of minor temperature fluctuation. As the effect from the temperature fluctuation is relative weak in comparison to the fluctuation induced by the locally applied microwave field. The discussion of spin waves propagation in magnonic waveguides as a function of temperature is beyond the scope of this article.

The numerically calculated dispersion relations of SWs in terms of the frequency f versus wavevector k for SMWs and BMWs under a bias field H = 100 mT with and without the presence of interfacial DMI are shown in Fig. 2. The equilibrium

magnetization in the positive and negative y direction is represented by P = +1 and -1, respectively. Without the presence of DMI, the dispersion relations of SWs are symmetric about zero wavevector indicating a reciprocal propagation property of SWs along the two opposite direction as shown in Figs. 2(a) and (b) for SMW and BMW, respectively. The frequencies and amplitudes of SWs with positive wavevector +k and negative wavevector -k are symmetric about the zero wavevector. For the SMW, there is a continuous quadratic dispersion and no forbidden band for frequencies above 10.5 GHz, which is the normal property of the DE SWs. For the BMW, the dispersion shows a periodic character of the two dispersion branches up to the second Brillouin zone (BZ), which is evident from Fig. 2(b). The dispersion curves are observed to be folded and feature bandgap with width of 13.6 GHz from 26.2 to 39.8 GHz at the BZ boundaries $k_x = \pi/a$, due to the periodic modulation of the magnetic properties along the SW propagation direction. This periodic character is typical of periodic systems such as magnonic band structure for the widely reported magnonic crystals. [28-30]

When considering the presence of the interfacial DMI, neither the continuous dispersion for SMW nor the magnonic dispersion for BMW is symmetrical about the zero wavevector indicating a nonreciprocal propagation property of SWs along the two opposite direction as shown in Figs. 2(c) and (e) for SMW and in Figs. 2(d) and (f) for BMW, respectively. The dispersion of SWs is shifted to the +k side for the magnetization P = +1. In contrast, the dispersion of SWs is shifted to the -k side when the magnetization P is reversed from +1 to -1. The shift of dispersion is equal for the same DMI constant with P = +1 and -1, similar to the reported results for an uniformly magnetized infinite planar film with the presence of interfacial DMI. [27] The interfacial DMI induced nonreciprocal dispersion depends not only on the wavevector direction but also on the magnetization direction. This DMI effect on the spin wave dispersion is similar to the Rashba spin-orbit coupling effect on electron dispersion since the interfacial DMI arises from the Rashba spin-orbit coupling at magnetic interfaces. [27, 42-45]

To better understand the dynamical properties of SWs *i.e.* frequencies, amplitudes, and mode profiles, we calculate the mode profiles of SWs at specific frequencies. The calculated mode profiles of SWs in magnonic waveguides without the presence of DMI are shown in Fig. 3 for two specific frequencies of 22 and 33 GHz, which are selected within the first allowed band and first bandgap of the BMW at **H** = 100 mT.

As shown in Fig. 3, for the two SWs in the SMW, the wavevector magnitudes and the amplitudes of the rightward (+*x*) propagating waves are the same as that of the leftward (-*x*) propagating waves. Therefore, the propagation of SWs are symmetrical or reciprocal in the rightward (with wavevector +*k*) and leftward (–*k*) directions. While the BMW only permits the propagation of the 22 GHz SW located in the first transmission band. For SW of 33 GHz located in the first bandgap of BMW is prohibited from propagation in the waveguide. Similar to the mode profiles of SWs in the SMW, the SWs in the BMW are also reciprocal.

The dispersion relations of the propagating SWs in the SMW with the presence of interfacial DMI are shown in Fig. 4(a), which clear shows the nonreciprocity of the SWs. To examine this nonreciprocal propagation in detail, we also calculate the associated nonreciprocity strength defined as the frequency difference between SWs propagating in rightward (+*k*) and leftward (-*k*) direction: $\Delta f(k) = f(+k) - f(-k)$, and the mode profiles of SWs with specific frequencies. The nonreciprocity strength is shown in Fig. 4(b), and it increases with the wavevector amplitudes, and reaches the maximal value of 18 GHz at $k \approx 0.204$ nm^{-1}.

The calculated mode profiles of SWs in SMW with the presence of DMI are shown in Fig. 4 insets for four specific frequencies of 12, 19, 26, and 40 GHz. The wavevector and frequency of the SW are referred to (***k***, *f*). As shown in Fig. 4, for the four SWs in the SMW, the wavevector magnitudes and the amplitudes of the rightward propagating waves are quite different from that of the leftward propagating waves, which is a clear signature of nonreciprocal SW propagation. As an instance, the rightward propagating 40 GHz SW has a wavevector magnitude of $1.27\pi/a$, which is larger than that of the leftward propagating 40 GHz SW $0.94\pi/a$. The SWs of the same wavevector magnitude propagating on the opposite directions have different frequencies by comparing the (-0.94, 40) and (0.94, 26) modes. Hence, the opposite propagating SWs in the SMW exhibit an obvious nonreciprocity property. In addition there exists unidirectional SW modes, which is only allowed to propagate only one direction, say rightward (+*k*), and is prohibited to propagate along the opposite (-*k*) direction, e.g., the mode profile of 12 GHz SW.

Fig. 5 shows the calculated dispersions and mode profiles of SWs in the BMW with the presence of interfacial DMI. This nonreciprocal magnonic band structure indicates the nonreciprocity property of propagating SWs in such waveguide. The

calculated nonreciprocity strength $\Delta f(k)$ is shown in Fig. 5(b), and the mode profiles of SWs with specific frequencies are shown in the insets of Fig. 5. In contrast to that for SMW, the nonreciprocity strength does not continuously increase with the wavevector amplitudes. A band structure like dispersion of nonreciprocity is observed, and it is enhanced when the rightward and leftward propagating SWs are located in the different frequency bands. For instance, the rightward propagating SW with $+k = \pi/a$ is located in the first band, while the leftward propagating SW with $-k = \pi/a$ is located in the second band. The nonreciprocity is enhanced as compared to the SWs in SMW with the same wavevector magnitude. The nonreciprocity can be as large as 37 GHz in the investigated range.

The calculated mode profiles of SWs in BMW with the presence of DMI are shown in Fig. 5 as insets for four specific frequencies of 14, 22, 33, and 41 GHz, which are selected within the first allowed band, first bandgap, and second allowed band of the BMW, respectively. The SW of 33 GHz is located in the first bandgap of the magnonic waveguide, so neither the rightward (-, 33) nor the leftward (+, 33) SW can propagate as shown in the mode profiles. For SWs with frequencies in the allowed bands, the wavevector magnitudes and the amplitudes of the rightward propagating waves are quite different from that of the leftward propagating waves indicating a nonreciprocal SW propagation. For instance, the rightward propagating 22 GHz SW has a wavevector magnitude of $1.15\pi/a$, which is larger than that of the leftward propagating 22 GHz SW $0.35\pi/a$. For the SWs of the same wavevector magnitude, (-0.74, 41) and (0.74, 14), they have different frequencies when they propagate in opposite directions. Hence, the SWs propagating along opposite direction in the BMW exhibit an obvious nonreciprocity property. Additionally, a narrow frequency range of unidirectional SW propagation is also observed from 10.2 to 14.8 GHz, in which the SWs propagate in the rightward and leftward directions are significantly different: the waveguide is transparent in the rightward direction and almost opaque in the leftwards direction, e.g., the mode profile of 14 GHz SW. This unidirectional property is reversible by reversing the magnetization direction to allow the leftward propagating SWs.

In summary, we demonstrate the nonreciprocity of spin waves in the nanostripe magnonic waveguides induced by the presence of the interfacial Dzyaloshinskii-Moriya interaction by micromagnetic simulations. The observed nonreciprocal

magnonic dispersion is attributed to the degeneracy breaking of the SWs propagating along the two opposite directions with the presence of the interfacial DMI. This nonreciprocal property of SWs with respect to the sign of the wavevector is demonstrated by calculating the spectra in both the positive and negative directions and by reversing the magnetization of the waveguides. Additionally, our simulation reveals the possibility of unidirectional spin wave propagation in a narrow frequency band of the magnonic dispersion where the propagation of SWs in the forward direction and backward direction is significantly different, *i.e.* the waveguide is transparent in the forward direction and opaque in the backward direction. Hence, our findings could inspire a new class of compact nonreciprocal magnonic devices releasing the isolation and dynamic control of spin wave propagation for future magnon-spintronic applications.

Reference

[1] I. E. Dzialoshinskii, Sov. Phys. **5**, 1259 (1957).
[2] T. Moriya, Phys. Rev. **120**, 91 (1960).
[3] A. Tonomura, X. Z. Yu, K. Yanagisawa, T. Matsuda, Y. Onose, N. Kanazawa, H. S. Park, and Y. Tokura, Nano. Lett. **12**, 1673 (2012).
[4] X. Z. Yu, N. Kanazawa, Y. Onose, K. Kimoto, W. Z. Zhang, S. Ishiwata, Y. Matsui, and Y. Tokura, Nat. Mater. **10**, 106 (2011).
[5] H. Wilhelm, M. Baenitz, M. Schmidt, U. K. Rößler, A. A. Leonov, and A. N. Bogdanov, Phys. Rev. Lett. **107**, 127203 (2011).
[6] X. Z. Yu, Y. Onose, N. Kanazawa, J. H. Park, J. H. Han, Y. Matsui, N. Nagaosa, and Y. Tokura, Nature **465**, 901 (2010).
[7] S. Mühlbauer, B. Binz, F. Jonietz, C. Pfleiderer, A. Rosch, A. Neubauer, R. Georgii, and P. Böni, Science **323**, 915 (2009).
[8] S. Heinze, K. VonBergmann, M. Menzel, J. Brede, A. Kubetzka, R. Wiesendanger, G. Bihlmayer, and S. Blügel, Nat. Phys. **7**, 713 (2011).
[9] M. Bode, M. Heide, K. von Bergmann, P. Ferriani, S. Heinze, G. Bihlmayer, A. Kubetzka, O. Pietzsch, S. Blügel, and R. Wiesendanger, Nature **447**, 190 (2007).
[10] G. Chen, J. Zhu, A. Quesada, J. Li, A. T. N Diaye, Y. Huo, T. P. Ma, Y. Chen, H. Y. Kwon, C. Won, Z. Q. Qiu, A. K. Schmid, and Y. Z. Wu, Phys. Rev. Lett. **110**, 177204 (2013).
[11] N. Kanazawa, Y. Onose, T. Arima, D. Okuyama, K. Ohoyama, S. Wakimoto, K. Kakurai, S. Ishiwata, and Y. Tokura, Phys. Rev. Lett. **106**, 156603 (2011).
[12] M. Lee, W. Kang, Y. Onose, Y. Tokura, and N. P. Ong, Phys. Rev. Lett. **102**, 186601 (2009).
[13] A. Neubauer, C. Pfleiderer, B. Binz, A. Rosch, R. Ritz, P. G. Niklowitz, and P. Boni, Phys. Rev. Lett. **102**, 186602 (2009).
[14] X. Z. Yu, N. Kanazawa, W. Z. Zhang, T. Nagai, T. Hara, K. Kimoto, Y. Matsui, Y. Onose, and Y. Tokura, Nat. Commun. **3**, 988 (2012).

[15] M. G. and A. R. F. Jonietz, S. Mühlbauer, C. Pfleiderer, A. Neubauer, W. Münzer, A. Bauer, T. Adams, R. Georgii, P. Böni, R. A. Duine, K. Everschor, Science **330**, 1648 (2010).
[16] J. Iwasaki and M. Mochizuki and N. Nagaosa, Nat. Commun. **4**, 1463 (2013).
[17] S. Emori, U. Bauer, S.-M. Ahn, E. Martinez, and G. S. D. Beach, Nat. Mater. **12**, 611 (2013).
[18] K.-S. Ryu, L. Thomas, S.-H. Yang, and S. Parkin, Nat. Nanotech. **8**, 527 (2013).
[19] G. Chen, T. Ma, A. T. N'Diaye, H. Kwon, C. Won, Y. Wu, and A. K. Schmid, Nat. Commun. **4**, 2671 (2013).
[20] A. Thiaville, S. Rohart, E. Ju_e, V. Cros, and A. Fert, Eur. Lett. **100**, 57002 (2012).
[21] A. T. Costa, R. B. Muniz, S. Lounis, A. B. Klautau, and D. L. Mills, Phys. Rev. B **82**, 014428 (2010).
[22] L. Udvardi and L. Szunyogh, Phys. Rev. Lett. **102**, 207204 (2009).
[23] D. cortes-Ortuno and P. Landeros, J. Phys.: Condens. Matter **25**, 156001 (2013).
[24] F. Garcia-Sanchez, P. Borys, A. Vansteenkiste, J.-V. Kim, and R. L. Stamps, Phys. Rev. B **89**, 224408 (2014).
[25] K. Zakeri, Y. Zhang, J. Prokop, T.-H. Chuang, N. Sakr, W. X. Tang, and J. Kirschner, Phys. Rev. Lett. **104**, 137203 (2010).
[26] Z. Kh, Z. Y, C. T-H, and K. J, Phys. Rev. Lett. **108**, 197205 (2012).
[27] J.-H. Moon, S.-M. Seo, K.-J. Lee, K.-W. Kim, J. Ryu, H.-W. Lee, R. D. McMichael, and M. D. Stiles, Phys. Rev. B **88**, 184404 (2013).
[28] M. Jamali, J. H. Kwon, S. M. Seo, K. J. Lee, and H. Yang, Sci. Rep. **3**, 3160 (2013).
[29] S. Neusser and D. Grundler, Adv. Mater. **21**, 2927 (2009).
[30] V. V. Kruglyak, S. O. Demokritov, and D. Grundler, J. Phys. D: Appl. Phys. **43**, 264001 (2010).
[31] B. Lenk, H. Ulrichs, F. Garbs, and M. Munzenberg, Phys. Rep. **507**, 107 (2011).
[32] M. Krawczyk and D. Grundler, J. Phys.: Condens. Matter **26**, 123202 (2014).
[33] W. L. Barnes, A. Dereux, and T. W. Ebbesen, Nature **424**, 824 (2003).
[34] D. K. Gramotnev and S. I. Bozhevolnyi, Nat. Photon. **4**, 83 (2010).
[35] V. E. Demidov, S. O. Demokritov, K. Rott, P. Krzysteczko, and G. Reiss, Appl. Phys. Lett. **92**, 232503 (2008).
[36] F. S. Ma, H. S. Lim, Z. K. Wang, S. N. Piramanayagam, S. C. Ng, and M. H. Kuok, Appl. Phys. Lett. **98**, 153107 (2011).
[37] F. S. Ma, H. S. Lim, V. L. Zhang, Z. K. Wang, S. N. Piramanayagam, S. C. Ng, and M. H. Kuok, J. Appl. Phys. **111**, 064326 (2012).
[38] R. W. Damon and J. R. Eshbach, J. Phys. Chem. Solids **19**, 308 (1961).
[39] *M. J. Donahue and D. G. Porter, OOMMF User's Guide, Version 1.2a5, http://math.nist.gov/oommf.*
[40] S. Rohart and A. Thiaville, Phys. Rev. B **88**, 184422 (2013).
[41] A. Thiaville, S. Rohart, E. Jue, V. Cros, and A. Fert, EPL **100**, 57002 (2012).
[42] A. T. Costa, R. B. Muniz, S. Lounis, A. B. Klautau, and D. L. Mills, Phys. Rev. B **82**, 014428 (2010).
[43] F. Schubert, Y. Mokrousov, P. Ferriani, and S. Heinze, Phys. Rev. B **83**, 165442 (2011).
[44] J.-H. Park, C. H. Kim, H.-W. Lee, and J. H. Han, Phys. Rev. B **87**, 041301(R) (2013).
[45] K.-W. Kim, H.-W. Lee, K.-J. Lee, and M. D. Stiles, Phys. Rev. Lett. **111**, 216601 (2013).

Figures

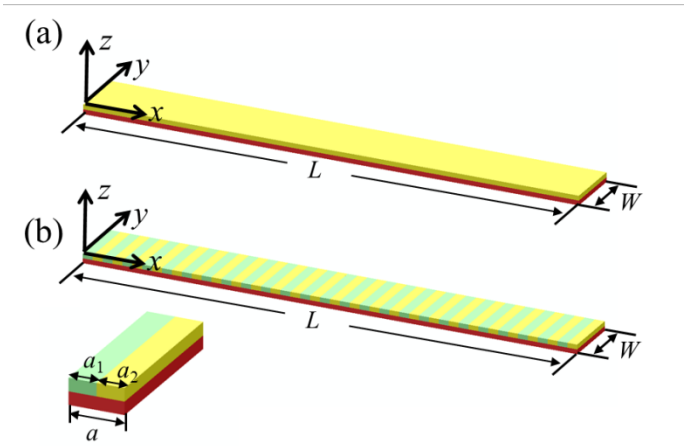

Fig. 1. (Color online) Schematic of the investigated magnonic waveguides: (a) single-component and (b) bi-component waveguide. The inset is the unit cell of the bi-component magnonic waveguide with the period $a = a_1 + a_2$ along the x-axis.

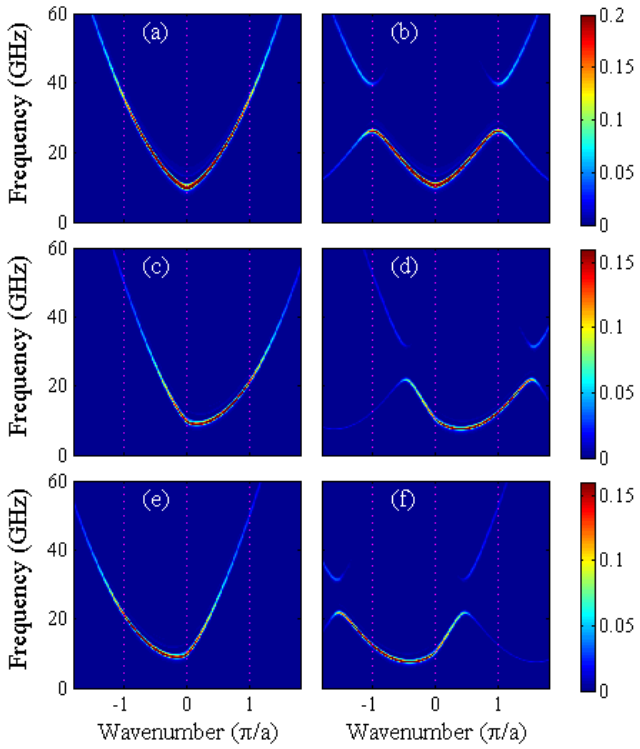

Fig. 2. (Color online) Dispersion relations of spin wave propagation in the single-component (left column) and bi-component (right column) magnonic waveguides under a magnetic field H = 100 mT for (a)-(b) D = 0, (c)-(d) D = 3 mJ/m^2 & P = +1, and (e)-(f) D = 3 mJ/m^2 & P = -1. The dotted lines indicate the Brillouin zone boundaries $k_x = n\pi/a$. The intensities of the spin waves are represented by the color scale.

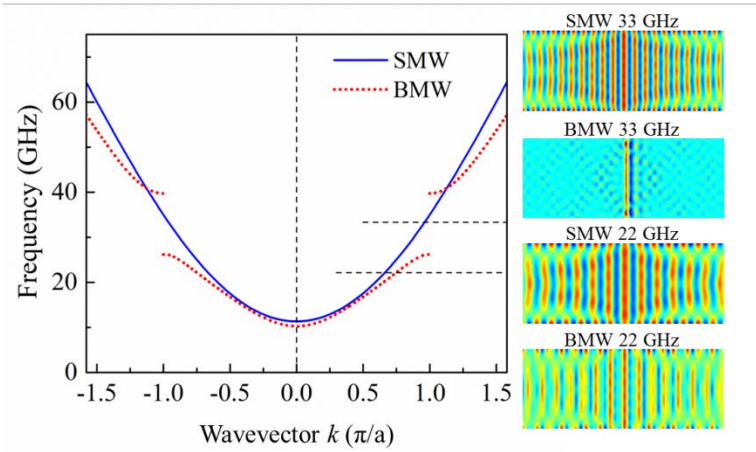

Fig. 3. (Color online) Fitted dispersion relations of spin wave propagation in the single-component (solid line) and bi-component (dotted line) magnonic waveguides under a magnetic field **H** = 100 mT for D = 0. The insets are the plane-view color-code images of the spin wave mode profiles obtained from a Fourier transform of the spatial distributions of the temporal evolution of the out-of-plane magnetization for various frequencies as labeled in the figure.

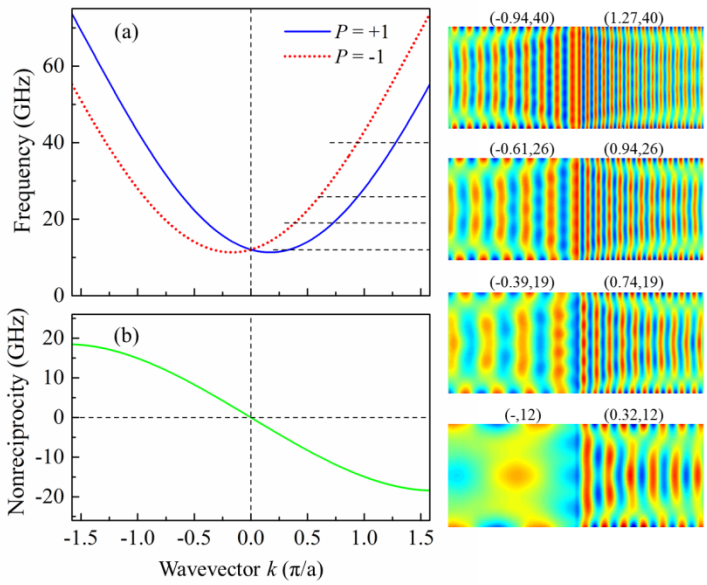

Fig. 4. (Color online) (a) Fitted dispersion relations of spin wave propagation in the single-component magnonic waveguides with D = 3 mJ/m^2 for the positive and negative magnetization. (b) The nonreciprocity strength defined as $\Delta f = f(k) - f(-k)$. The insets are the plane-view color-code images of the spin wave mode profiles obtained from a Fourier transform of the spatial distributions of the temporal evolution of the out-of-plane magnetization for various frequencies as labeled in the Fig. 4(a).

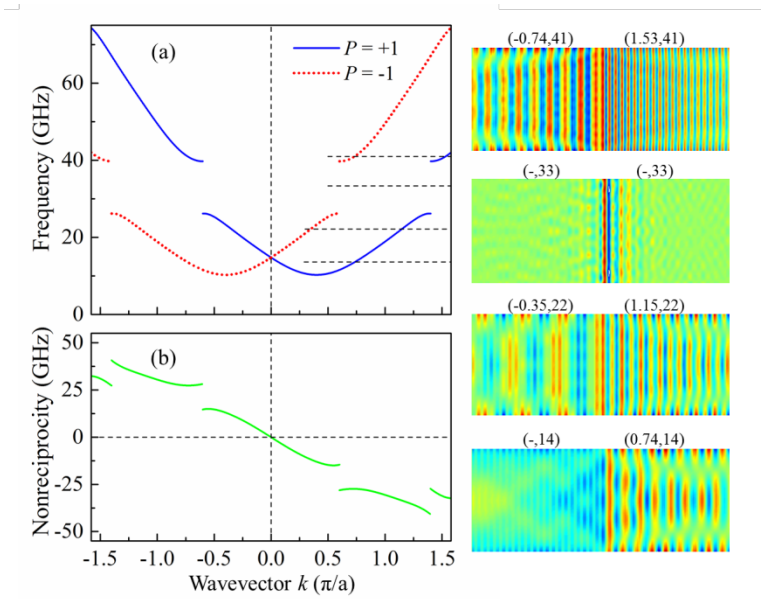

Fig. 5. (Color online) (a) Fitted dispersion relations of spin wave propagation in the bi-component magnonic waveguides with D = 3 mJ/m^2 for the positive and negative magnetization. (b) The nonreciprocity strength defined as $\Delta f = f(k) - f(-k)$. The insets are the plane-view color-code images of the spin wave mode profiles obtained from a Fourier transform of the spatial distributions of the temporal evolution of the out-of-plane magnetization for various frequencies as labeled in the Fig. 5(a).